Sensing of Surface Strain with Flexible Fiber Bragg Strain Gages

Jochen Maul and Tobias Kipp

HBM GmbH, Im Tiefen See 45, 64293 Darmstadt, Germany
Emails: jochen.maul@hbm.com, tobias.kipp@hbm.com

Chapter 7-9

---

7. Calibration of Optical Interrogators

For calibration of optical interrogators, athermal fiber Fabry Perot etalons are used as an absolute wavelength scale.

The etalon basically consists of two fixed plane-parallel dielectric surfaces which are inserted into the fiber path. They act as a precision wavelength filter through multiple reflections and interference of light rays from the partially reflecting dielectric surfaces. Etalon reflection peaks are described by the Airy function

$$R(\lambda) \propto \left(1 + F \sin^2(\delta/2)\right)^{-1} \tag{18}$$

where the optical phase acquired by the light wave on one round trip through the etalon is given by $\delta = 4\pi n l/\lambda$. Here, n is the index of refraction and l is the distance between both etalon interfaces. The finesse $F = 4R/(1-R)^2$ with the dielectric surface reflectivity R is used to quantify the shape of the etalon reflection peaks. The Free Spectral Range (FSR) $\Delta\lambda$ displays the peak-to-peak distance.

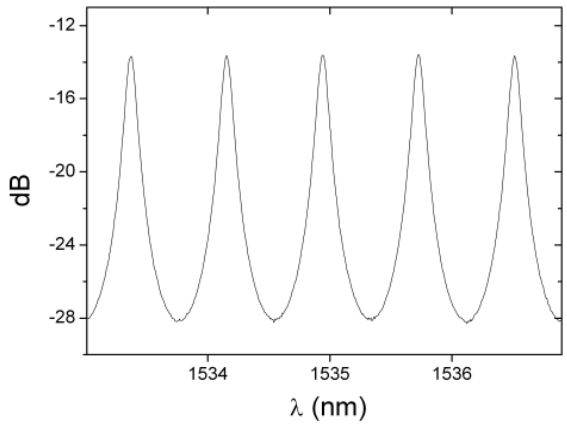

Fig. 15. Section of the fiber etalon reflection spectrum used for interrogator calibration.

Fig. 15 shows a small section of the fiber etalon reflection spectrum recorded by a HBM SI401 interrogator. The etalon peaks are remarkably sharp and therefore precisely define a broad spectrum of calibration wavelengths. They do not change their position with temperature and they cover the complete interrogation range between 1510 and 1590nm. In the zoomed etalon spectrum of **Fig. 15** the FSR is ~0.8nm around λ_0~1535nm.

By peak wavelengths determination using HBM interrogators which are actively calibrated using an implemented gas cell standard (e.g. the HBM SI401), an absolute calibration of the etalon is performed. This procedure allows to establish a calibration protocol by listing the etalon peak wavelengths measured with a certified gas cell interrogator together with the etalon peaks measured with the interrogator in quest.

For both static and dynamic interrogators, the absolute calibration error is below 10pm (typically ±1-2pm).

8. Anomalies in the Bragg Spectrum

a. Birefringence and Inhomogeneous Strain

In this chapter, some basic effects are described which might lead to failure in Bragg peak recognition or even falsify the Bragg signal.

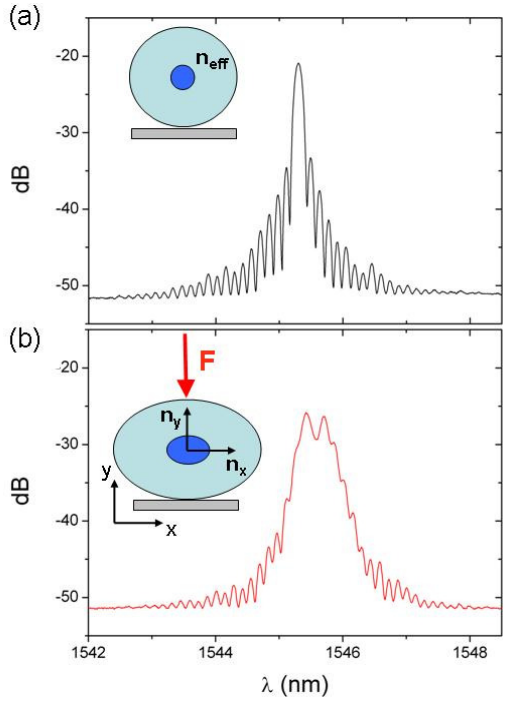

Fig. 16. Bragg spectrum (a) without and (b) in the presence of birefringence. The insets illustrate the change in the core refractive index (a) without and (b) with a transverse force applied to the fiber.

A major source for deficient signal detection is *birefringence* [14]:
Radial forces F per fiber length L (F/L) lead to anisotropic refractive indices n_{eff}^{x} and n_{eff}^{y} in the fiber core (**Fig. 16**). This effects a splitting of the Bragg peak into two separate peaks:

(19) $\lambda_B^i = 2\, n_{eff}^i (F/L)\, \Lambda \quad (i = x, y)$

The difference between both refractive indices defines the birefringence β

(20) $\beta := n_{eff}^{x} - n_{eff}^{y}$

which directly measures the magnitude of Bragg peak splitting:
(21) $\Delta\lambda_B(F/L) = 2\,\Lambda\,\beta(F/L)$

For the Bragg fiber used in all above sensors, we find experimentally

(22) $\beta \approx 3.15 * 10^{-7}\, (F/N)/(L/mm)$.

Fig. 16 shows an unperturbed Bragg peak as well as a double peak due to birefringence. Obviously, birefringence causes an ambiguity in the peak identification process in which the

wavelength at peak maximum is depicted. In practice, birefringence may be caused e.g. either by change of the glue properties or by direct application of radial forces.

Strongly inhomogeneous strain profiles may cause a broadening or splitting of the Bragg peak as well: in contrast to electric strain gages, strain affects the Bragg grating *locally* and does not necessarily sum up to a uniform signal peak. This means that a strongly inhomogeneous strain profile, such as e.g. due to microcracks directly underneath the bonded Bragg grating, results in a series of adjacent Bragg peaks.

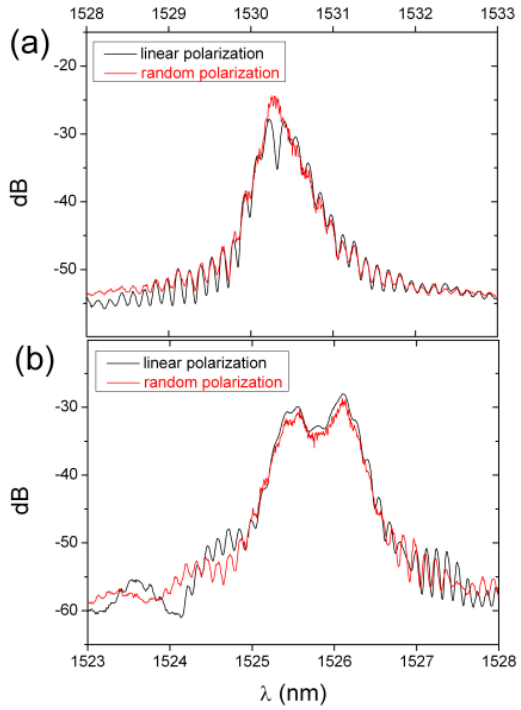

Fig. 17. Bragg signal deformation in the presence of (a) *birefringence* and (b) *inhomogeneous strain profile*.
To distinguish both cases, the Bragg signal was measured with linear and random light polarization. Whereas birefringence only shows peak splitting by using linearly polarized light for interrogation, inhomogeneous strain interrogation is not affected by light polarization.

In this case, the Bragg spectrum is obtained from the Bragg signal average over the spatial strain profile $\varepsilon(z)$ within the grating length L:

$$R(\lambda) \propto \int_L R(\lambda, z)\, dz \qquad (23)$$

Here, $R(\lambda, z)$ is derived from eqn. (3) by introducing a spatial strain dependence of the grating period Λ,

$$\Lambda \equiv \Lambda(z) = \Lambda_0\, \varepsilon(z) + \Lambda_0 . \qquad (24)$$

Here, Λ_0 is the period of the unstrained grating. In this sense, the variable $x(\lambda)$ in eqn. (3) becomes $x(\lambda, z) = \pi N \left(\lambda - 2n_{eff}\Lambda(z)\right) / \left(2n_{eff}\Lambda(z)\right)$, yielding $R(\lambda, z) \equiv \left|\sin(x(\lambda, z)) / x(\lambda, z)\right|$.

To distinguish birefringence from inhomogeneous strain experimentally, an optical scrambler (General Photonics PCD-104) was used to generate random light polarization from the linear light polarization of the interrogator: Since the Bragg wavelength is only sensitive to different anisotropic refractive indices n_{eff}^{x} and n_{eff}^{y} in the presence of *linearly* polarized light, randomization of polarization states leads to the detection of a uniform Bragg peak (**Fig. 17a**).

In contrast, Bragg signals from inhomogeneous strain profiles do not depend on the polarization state of light (**Fig. 17b**).

Strongly **inhomogeneous strain** profiles underneath the Bragg grating resp. **lateral fiber forces** can significantly distort the Bragg peak shape and lead to peak detection problems.

b. *Background Modulations from Fiber Ends*

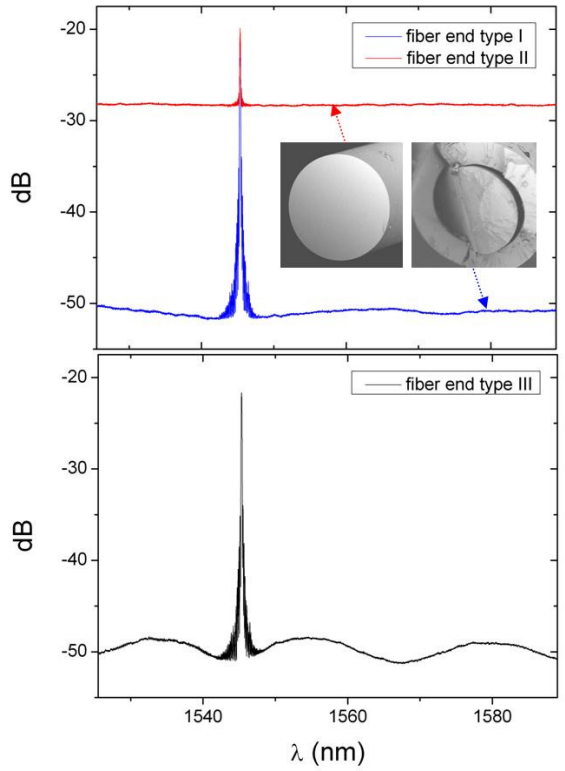

Fig. 18. Backgrounds modulations of the Bragg spectrum. Three types (I-III) are distinguished depending on the morphology of the fiber end. Insets: SEM micrographs of fiber ends attributed to aberrant background modulation of types I and II, as detailed in the text.

Further, the shape of the Bragg fiber *end* influences the signal-to-background ratio because it determines the degree of unselective back-reflection. **Fig. 18.** shows background levels relative to the Bragg peak for different fiber end configurations.

Type I represents an irregular fiber cut with diffuse light reflection at the end for which the lowest background level is obtained. In contrast, type II represents a 0° cut end. Here, ~4% of laser light is reflected back into the fiber at any wavelength and superimposes the Bragg spectrum. In the case of type III, the formation of at least one mirror facet in a small angle to the fiber core likely leads to an interferometric arrangement of the ends of both measurement fiber and coupler fiber (see **Fig. 18**, dotted frames). The period of the resulting background oscillation appears therefore characteristic for the fiber cutting angles.

Since **background modulations** stem from regular **fiber end cuts**, they can be avoided in practise by irregular cuts and subsequent sealing of the fiber ends.

9. Applications

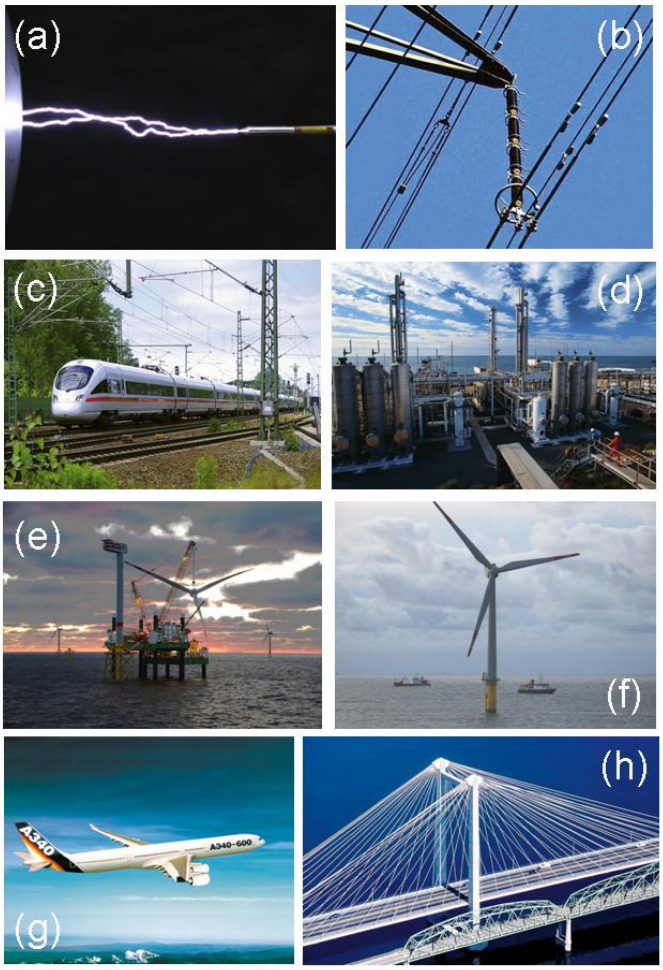

Fig. 19. Possible applications for optical strain gage technology as discussed in the text.

A major advantage of optical against electrical strain gages is the immunity with respect to electrical influences, such as illustrated in **Figs. 19a-c**, i.e. during discharges (**Fig. 19a**; optical strain gage K-OL installed on an electrode) or in high voltage wiring (**Fig. 19b**) as well as in electrical grounding as present in rails (**Fig. 19c,** see also e.g. [15]). **Fig. 19d** shows a typical environment in chemical industry where explosion detection might be required. Here, optical strain gages are preferable because they need no electric current at the inspection areas. Humidity is an important aspect in off-shore applications such as in **Fig. 19e**. Water penetration usually leads to failure (short circuits) in electrical sensors but not in optical gages. Also, optical gages are less accessible to corrosion by sea water. High strain levels often occur in wind energy rotor blades (**Fig. 19f**) and in aerospace applications (**Fig. 19g**) where fiber reinforced plastics are in use. In this case the high tensile strength of the Bragg fiber is beneficial. For survey of longer distances such as on bridges (**Fig. 19h**), the optical measurement chain avoids strong cabling efforts and cable costs because a single fiber can contain multiple sensors.

References

[1] Ch.K. Kao, Optical fiber technology, IEEE Press, New York, USA (1981);
The Nobel Prize in Physics 2009 – Press Release, Nobel Foundation, http://nobelprize.org/nobel_prizes/physics/laureates/2009/press.html;

[2] P.S. Theocaris, Moiré fringes in strain analysis, Pergamon (1969).

[3] R.P. Khetan and F.P. Chiang, Strain analysis by one-beam laser speckle interferometry, Appl. Opt. 15, 2205-2215 (1976).

[4] C. Belleville and G. Duplain, White-light interferometric multimode fiber-optic strain sensor, Opt. Lett. 18, 78-80 (1993).

[5] P.B. Tarsa, M. Brzozowski, P. Rabinowitz, and K.K. Lehmann, Cavity ringdown strain gauge, Opt. Lett. 29, 1339-1341 (2004).

[6] D. Graham-Rowe, Sensors take the strain, Nat. Photon. 1, 307-309 (2007).

[7] K.O. Hill, Y. Fujii, D. C. Johnson, and B. S. Kawasaki, Photosensitivity in optical fiber waveguides: application to reflection fiber fabrication, Appl. Phys. Lett. 32, 647-649 (1978).

[8] G. Meltz, W.W. Morey, and W.H. Glenn, Formation of Bragg gratings in optical fibers by a transverse holographic method, Opt. Lett. 14, 823-825 (1989).

[9] E. Brinkmeyer, „Faseroptische Gitter“, in: Optische Kommunikationstechnik, Eds. E. Voges and K. Petermann, Springer (2002).

[10] M.W. Rothhardt, C. Chojetzki, and H.R. Müller, High-mechanical-strength single-pulse draw tower gratings, Proc. SPIE 5579, 127 (2004).

[11] M. Kreuzer, Strain Measurement with Fiber Bragg Grating Sensors (2007), online at www.hbm.com .

[12] A. Bertholds and R. Dändliker, Determination of the individual strain optic coefficients in single mode optical fibers, J. Lightwave Tech. 6, 17-20 (1988).

[13] K. Hoffmann, An Introduction to Measurements using Strain Gages, HBM (1987).

[14] J. Zhao, X. Zhang, Y. Huang, and X. Ren, Experimental analysis of birefringence effects on fiber Bragg gratings induced by lateral compression, Opt. Commun. 229, 203-207 (2004).

[15] W. Lee, J. Lee, C. Henderson, H.F. Taylor, R. James, C.E. Lee, V. Swenson, R.A. Atkins, and W.G. Gemeiner, Railroad bridge instrumentation with fiber-optic sensors, Appl. Opt. 38, 1110-1114 (1999).